PCCP

View Online
Dynamic Article Links

Cite this: *Phys. Chem. Chem. Phys.*, 2011, **13**, 8671–8680

www.rsc.org/pccp

PAPER

Laser-induced alignment and anti-alignment of rotationally excited molecules

Nina Owschimikow,*[a] Burkhard Schmidt[b] and Nikolaus Schwentner[a]

Received 25th October 2010, Accepted 22nd December 2010
DOI: 10.1039/c0cp02260h

We numerically investigate the post-pulse alignment of rotationally excited diatomic molecules upon nonresonant interaction with a linearly polarized laser pulse. In addition to the simulations, we develop a simple model which qualitatively describes the shape and amplitude of post-pulse alignment induced by a laser pulse of moderate power density. In our treatment we take into account that molecules in rotationally excited states can interact with a laser pulse not only by absorbing energy but also by stimulated emission. The extent to which these processes are present in the interaction depends, on the one hand, on the directionality of the molecular angular momentum (given by the M quantum number), and on the other hand on the ratio of transition frequencies and pulse duration (determined by the J number). A rotational wave packet created by a strong pulse from an initially pure state contains a broad range of rotational levels, over which the character of the interaction can change from non-adiabatic to adiabatic. Depending on the laser pulse duration and amplitude, the transition from the non-adiabatic to the adiabatic limit proceeds through a region with dominant rotational heating, or alignment, for short pulses and a large region with rotational cooling, and correspondingly preferred anti-alignment, for longer pulses.

1. Introduction

In recent years, the light-induced manipulation and control of the rotational state of diatomic molecules with polarized laser pulses has developed into an important topic, in experiment[1,2] as well as in theory.[3] The interaction of molecule and laser electric field leads to the formation of an anisotropic distribution of molecular axes. Interaction with a laser pulse which is very long compared to the molecular rotational period is termed adiabatic interaction. It results in the formation of pendular states,[4–7] which are eigenstates for the combined molecule–field system reflecting the cylindrical symmetry of the problem. During the slow turn-off of the laser pulse, the adiabatically aligned ensemble returns to the original isotropic distribution. For very short laser pulses, the non-adiabatic alignment in the laser polarization direction is, apart from a small permanent term, transient and oscillates between alignment and anti-alignment in a rotational wave packet motion.[8,9] This field-free alignment[8] following the non-adiabatic excitation plays an important role in experiments studying direction-dependent properties of molecules.[10–19]

Analytical approaches to the calculation of molecular alignment dynamics are restricted to either the impulsive or the classical cases of alignment in the rotational ground state due to the prohibitive algebraic complexity of the problem.[20,21] In this case, anti-Stokes processes as well as the directionality of the molecule with respect to the laser field are irrelevant. Beyond this, the theoretical study of rotational alignment dynamics is largely based on numerical solution of the time-dependent Schrödinger equation (TDSE). The existence of rotational anti-Stokes as well as Stokes transitions has been used to fine-tune molecular energy levels.[22] Additionally, both non-adiabatic and adiabatic limiting cases have been studied and compared in the literature[23,24] for the thermal ensemble.

In the present contribution we identify the physical processes shaping the interaction of a rotationally excited diatomic molecule with a linearly polarized laser pulse of arbitrary duration. We systematically investigate the effects of directionality, pulse duration and pulse power on the rotational transitions. With the results, an analytical empirical model is developed, which allows one to predict the outcome of an alignment experiment for finite temperatures and pulse durations without resorting to full scale numerical simulations. This extends our previously published results[25] by accounting for anti-Stokes – as well as for Stokes – processes in the interaction of molecule and field. The basic considerations regarding the influence of the M quantum number and the non-adiabatic to adiabatic transition stay valid also for the interaction with strong laser

[a] *Institut für Experimentalphysik, Freie Universität Berlin, Arnimallee 14, 14195 Berlin, Germany. E-mail: nina.owschimikow@fu-berlin.de, nikolaus.schwentner@fu-berlin.de*
[b] *Institut für Mathematik, Freie Universität Berlin, Arnimallee 6, 14195 Berlin, Germany. E-mail: burkhard.schmidt@fu-berlin.de*

pulses. A rotational wave packet created by a strong pulse from an initially pure state contains a broad range of rotational levels. While the non-adiabatic to adiabatic transition for a weak interaction selects a density packet in a part of the thermal ensemble,[25] in the strong field case it can shape the energy content of a wave packet. For short pulses, the well-known rotational heating, corresponding to an increase in the overall alignment is obtained. In the transition to the adiabatic regime, counter-intuitively, for longer pulses there appears a crossover to preferred rotational cooling, or anti-alignment.

To illustrate our points, we perform numerical simulations on the $^{14}N_2$ molecule. To provide a better insight regarding the physical processes involved in the molecular alignment, much of the discussion in the following is based on rotational wave packets originating from an initially pure state. These effects become accessible in experiments due to the recent progress in the alignment of quantum state-selected molecules[17,18] and the possibility of state-resolved detection.[26,27]

2. Simulation methods

The rotation of a diatomic molecule in the rigid rotor approximation is governed by the Hamiltonian

$$H_0 = B\boldsymbol{J}^2 \text{ with } H_0|J,M\rangle = BJ(J+1)|J,M\rangle, \quad (1)$$

where $\boldsymbol{J}$ denotes the angular momentum operator with eigenvalues $J(J+1)$ characteristic of the rotational energy, and B is the rotational constant of the molecule. To induce alignment in an ensemble of molecules, usually laser pulses with frequencies in the visible or near-infrared region are employed. Except for the light H_2 molecule,[28] the rapid oscillations of the electric field are too fast for the nuclei to follow, and the interaction is mediated by the electronic polarizability α of the molecule. For a linearly polarized laser pulse with a non-resonant frequency much greater than the inverse of the laser pulse duration, the potential a diatomic molecule experiences is obtained by averaging over the pulse period and is described as[4,5]

$$H_{\text{ind}}(\theta,t) = -\tfrac{1}{4}\Delta\alpha E^2(t)\cos^2\theta - \tfrac{1}{4}\alpha_\perp E^2(t), \quad (2)$$

where $E(t)$ is the amplitude of the laser electric field, θ is the angle the molecular axis forms with the polarization direction of the laser, and $\Delta\alpha = \alpha_\parallel - \alpha_\perp$ is the anisotropy of polarizability given by the difference of α parallel to the molecular axis and $\alpha_\perp$ perpendicular to it. The complete Hamiltonian describing the nonresonant molecule-field interaction is the sum of the induced potential H_{ind} and the free rotor Hamiltonian H_0,

$$H(t) = H_0 + H_{\text{ind}}(t). \quad (3)$$

Fig. 1 shows a comparison of the J-dependent rotational energy given as $BJ(J+1)$ (solid circles) with the interaction potential $\Delta\alpha E^2/4$ created by a laser with power densities between 10 TW cm^{-2} and 100 TW cm^{-2}. For nitrogen, one has $B = 1.989$ cm^{-1} (ref. 29), and $\Delta\alpha = 0.78$ Å^3 (ref. 30). Up to the rotational level $J = 5$, $J = 14$, and $J = 19$ for power densities of 10, 5, and 100 TW cm^{-2}, respectively, the molecules can be efficiently trapped and aligned in the laser field under steady-state conditions. Note that few 100 TW cm^{-2}, depending on the pulse duration and the particular molecule, are the limit of experimentally applicable field strength, beyond which the ionization probability cannot be neglected.[31,32]

The rotational quantum state of a molecule during the interaction with the laser is usually expanded in terms of free rotor states $|J',M'\rangle$ as

$$|\Psi_{JM}(t)\rangle = \sum_{J'M'} c^{(JM)}_{J'M'}(t)|J',M'\rangle \quad (4)$$

where the quantum numbers J' and M' are the angular momentum quantum number and its projection onto the laser field direction. The indices JM denote the initial pure rotational state with $c^{(JM)}_{J'M'}(t=0) = \delta_{JJ'}\delta_{MM'}$. The corresponding probability density for the wave packet is expressed as

$$\rho_{JM}(t) = |\Psi_{JM}(t)\rangle\langle\Psi_{JM}(t)|. \quad (5)$$

In our simulations we numerically solve the TDSE for all $|\Psi_{JM}(t)\rangle$ using the Wave Packet 4.7 software package.[33]

The alignment of a diatomic molecule is usually quantified by the expectation value of the squared alignment cosine $\cos^2\theta$ of the angle between molecular axis and laser pulse polarization direction. This is also the quantity measured in optical Kerr effect or transient grating experiments.[34–37] The full angular distribution is recovered in the Coulomb-explosion based detection of the distribution of molecular fragments, see *e.g.* ref. 12 and 38 and may reveal a more detailed picture of rotational density packet. Here, we restrict the discussion to the expectation value of the squared cosine.

In our notation, the expectation value $\langle\cos^2\theta\rangle_{JM}$ describes the mean alignment of a wave packet, as the dynamics originate solely from the coherent superposition of rotational transitions excited in the molecule-field interaction of one originally pure state $|J,M\rangle$. In contrast, $\langle\langle\cos^2\theta\rangle\rangle_J$ represents the mean alignment averaged over all wave packets originating from the same rotational level J with equally weighted M-states. The corresponding density packet can be written as incoherent averaging with

$$\rho_J(t) = \frac{1}{2J+1}\sum_{M=-J}^{J}\rho_{JM}(t). \quad (6)$$

The outcome for averaging over all M states for a given J corresponds to a directional mean. Thermal averaging over all J results in an additional energetic smoothing. The mean alignment of a thermal density packet is represented as $\langle\langle\cos^2\theta\rangle\rangle_T$. The time-dependent density in this case is expressed as

$$\rho_T(t) = \sum_J w_T(J)\rho_J(t), \quad (7)$$

with the distribution of the coefficients $w_T(J)$ given by the thermal Boltzmann distribution and nuclear spin effects as

$$w_T(J) = \frac{w_I(J)(2J+1)e^{-BJ(J+1)/k_BT}}{\sum_J w_I(J)(2J+1)e^{-BJ(J+1)/k_BT}}. \quad (8)$$

The degeneracy $w_I(J)$ of even rotational states for the case of $^{14}N_2$ with nuclear spin $I = 1$ is twice as high as for odd

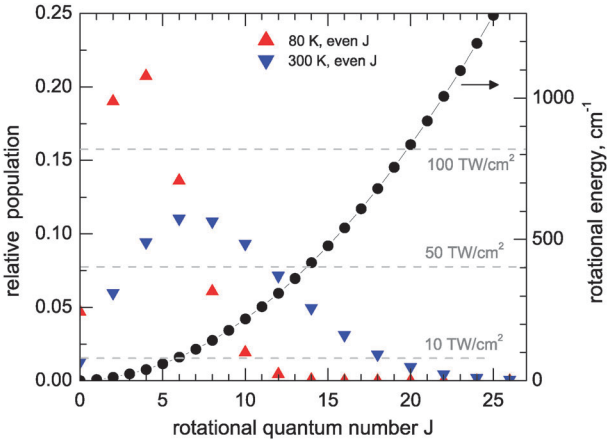

Fig. 1 Population of even rotational levels for $^{14}N_2$ at 80 K (▲) and 300 K (▼) and the corresponding rotational energy $BJ(J+1)$ (●). For comparison, the barrier heights $\Delta\alpha E^2/4$ created by laser power densities of 10, 50, and 100 TW cm^{-2} are shown as dashed gray lines.

rotational states.[39] The thermal distribution of population of even rotational levels is shown in Fig. 1 for 80 K and 300 K. At room temperature, the peak of the distribution is located around the $J = 8$ rotational level. Hence, we use the $J = 8$ rotational level to exemplify many of our considerations in the following. This affects the numerical values of amplitudes, probabilities, and other quantities. The general picture, however, remains valid for all rotational levels, because the dimensionless ratio of molecular rotational period to laser pulse duration turns out to be the determining parameter.[25]

3. Directionality effects

A rotational state J, when measured with respect to a space-fixed axis z, appears to be $(2J+1)$-fold degenerate, with the substates characterized by the quantum number M. The wave function for every of the M-states projected onto the z-axis displays a different mean alignment. Fig. 2 shows the mean alignments

$$p^0_{JM} \equiv \langle\cos^2\theta\rangle = \langle JM|\cos^2\theta|JM\rangle = \frac{1}{3} + \frac{2}{3}\frac{J(J+1)-3M^2}{(2J+3)(2J-1)} \quad (9)$$

from $M = 0$ to $M = 8$ onto the laser polarization direction.[40] For constant M, corresponding to the selection rule $\Delta M = 0$ for states coupled in the interaction with a linearly polarized laser, the curves are monotonically increasing functions of J, approaching a common limit of 1/2. The only exception is the curve for $M = 0$, which overshoots at small J and returns to 1/2. For all rotational states one has

$$\langle\langle\cos^2\theta\rangle\rangle_J = \frac{1}{2J+1}\sum_{M=-J}^{J}\langle\cos^2\theta\rangle_{JM} = \frac{1}{3}. \quad (10)$$

Rotationally excited molecules can exchange energy with the laser field by absorption and by stimulated emission in Stokes and anti-Stokes processes. A $\Delta J = +2$, $\Delta M = 0$ rotational transition leads to an increase in the mean alignment because of the increase in $\langle\cos^2\theta\rangle_{JM}$ for constant M and also because the highest M states cannot be populated. In the following, we refer to this ascent of the ladder of rotational states as an aligning transition. Classically, this corresponds to a narrowing of the cone which the molecular axis forms with the field polarization direction and at the same time an acceleration of the motion in the direction of the field vector, caused by the increase in rotational energy, as displayed in the left inset of Fig. 2.

The $\Delta J = -2$, $\Delta M = 0$ rotational transition, on the other hand, decreases the mean alignment. This descent on the J-ladder will be referred to as anti-aligning transition. Classically, the molecule loses rotational energy to the field, and the axis moves away from the polarization direction into anti-alignment, see right inset of Fig. 2.

The matrix elements for the ascending and descending transitions to the $J+2$ and the $J-2$ rotational levels, respectively, are given by ref. 40 as

$$p^+_{JM} \equiv \langle J,M|\cos^2\theta|J+2,M\rangle = \frac{\sqrt{(J+1+M)(J+2-M)(J+1+M)(J+2+M)}}{(2J+3)\sqrt{(2J+1)(2J+5)}}, \quad (11)$$

$$p^-_{JM} \equiv \langle J,M|\cos^2\theta|J-2,M\rangle = \frac{\sqrt{(J-1-M)(J-M)(J-1+M)(J+M)}}{(2J-1)\sqrt{(2J-3)(2J+1)}}. \quad (12)$$

These matrix elements show a dependence very similar to the diagonal ones plotted in Fig. 2, rising for constant M from a certain minimal value asymptotically to 1/2. Fig. 3 shows the ratio p^+_{JM}/p^-_{JM} from $J = 2$ to $J = 8$. The transition to the higher rotational state is favored because of the preference of p^+_{JM}, and thus alignment is most pronounced for $J \approx M$. An exception is again the case of $M = 0$, where the curve is essentially J-independent after an initial increase.

The ensemble-averaged squared alignment cosine is expressed in terms of the coefficients of the wave function according to eqn (4) and the projection matrix elements according to eqn (11) and (12) as

$$\langle\langle\cos^2\theta\rangle\rangle_T(t) = \sum_{\substack{J'M'\\J''M''}}\langle J'M'|\cos^2\theta|J''M''\rangle \times \sum_{JM} w_T(J)\rho^{(JM)}_{J'M'J''M''}(t), \quad (13)$$

where $w_T(J)$ is given by eqn (8), and

$$\rho^{(JM)}_{J'M'J''M''}(t) = (c^{(JM)}_{J''M''}(t))^* c^{(JM)}_{J'M'}(t)|J''M''\rangle\langle J',M'|. \quad (14)$$

For the coefficients of the freely evolving wave packet after the termination of the laser pulse at time t_f one has

$$c^{(JM)}_{J'M'}(t>t_f) = c^{(JM)}_{J'M'}(t_f)e^{i\frac{B}{\hbar}J'(J'+1)(t-t_f)}. \quad (15)$$

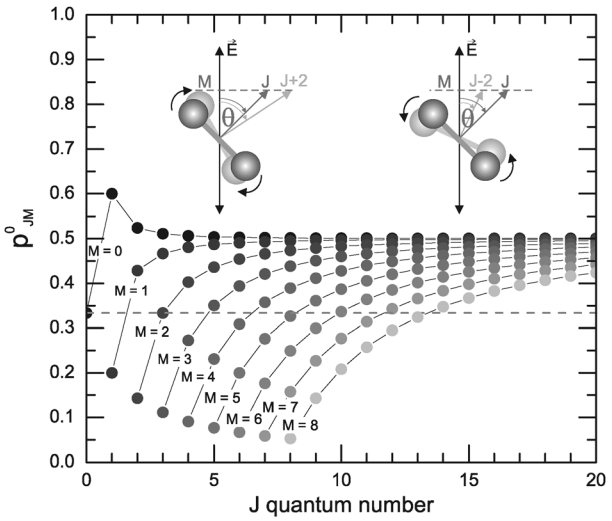

Fig. 2 Plot of the diagonal elements of the $\cos^2\theta$-matrix $p^0_{JM} = \langle J,M|\cos^2\theta|J,M\rangle$ (eqn (9)) from $M = 0$ to $M = 8$. The dashed horizontal line represents the average value of 1/3. Left inset: Increase in molecular alignment upon a $\Delta J = +2$, $\Delta M = 0$ transition. Right inset: Decrease of alignment in a $\Delta J = -2$, $\Delta M = 0$ transition.

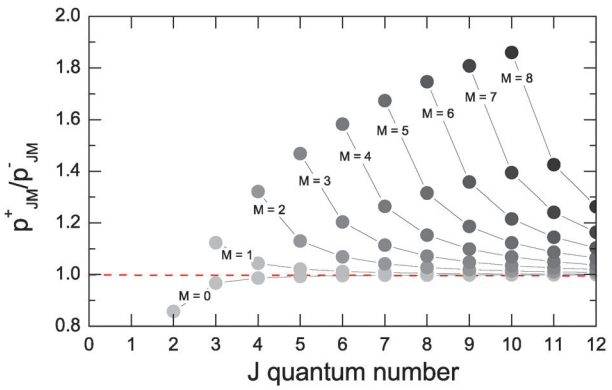

Fig. 3 Ratio of transition probabilities p^+_{JM}/p^-_{JM} to the $J + 2$ and $J - 2$ rotational levels for $2 < J < 8$. Equal probability is represented by the dashed horizontal line.

Using eqn (10)–(12) and the mean alignment of a thermal distribution of rotational states, eqn (13) can be rewritten as

$$\langle\langle\cos^2\theta\rangle\rangle_T(t) = \sum_{J'M'} p^0_{J'M'} \sum_{JM} w_T(J)\rho^{(JM)}_{J'M'J'M'}(t_f) + \sum_{\substack{J'M' \\ J+2,M'}} p^+_{J'M'} e^{-i\frac{B}{\hbar}(4J'+6)(t-t_f)} \sum_{JM} w_T(J)\rho^{(JM)}_{J'M'(J'+2)M'}(t_f) + \sum_{\substack{J'M' \\ J-2,M'}} p^-_{J'M'} e^{i\frac{B}{\hbar}(4J'+2)(t-t_f)} \sum_{JM} w_T(J)\rho^{(JM)}_{J'M'(J'-2)M'}(t_f) \quad (16)$$

Here, the time-independent first term gives the temporal average, about which the alignment is oscillating. The frequencies contributing to the time-dependent signal are

$$-B(4J' + 6) \text{ for } \Delta J = +2 \text{ and} \quad (17)$$

$$B(4J' - 2) \text{ for } \Delta J = -2 \quad (18)$$

Note that Stokes- and anti-Stokes transitions contribute with opposite sign to the time-dependent alignment dynamics.

The post-pulse alignment observed in a ρ_{JM} rotational wave packet upon the non-adiabatic excitation with a short laser pulse of moderate power density is exemplified in Fig. 4(a) using the ρ_{80}, ρ_{86}, and ρ_{88} rotational wave packets. Plotted are the time-dependent squared alignment cosines $\langle\cos^2\theta\rangle_{JM}$ for the corresponding wave functions. According to Fig. 3, the observed dynamics should show some directionality-dependent peculiarities. For the ρ_{80} wave packet, the transition probabilities for $\Delta J = +2$ and $\Delta J = -2$ transitions are almost identical. For the case of ρ_{86}, the ratio of transition matrix elements is 1.7, favoring the $\Delta J = +2$ rotational transition. The resulting alignment pattern for the ρ_{80} and ρ_{86} wave packets is thus a beating of two oscillations, the frequencies of which are given by the transition energies of 75. 6 cm^{-1} to the $J = 10$ and 59.7 cm^{-1} for the $J = 6$ rotational levels. The rotational periods for these transitions are 0.441 and 0.559 ps, respectively.

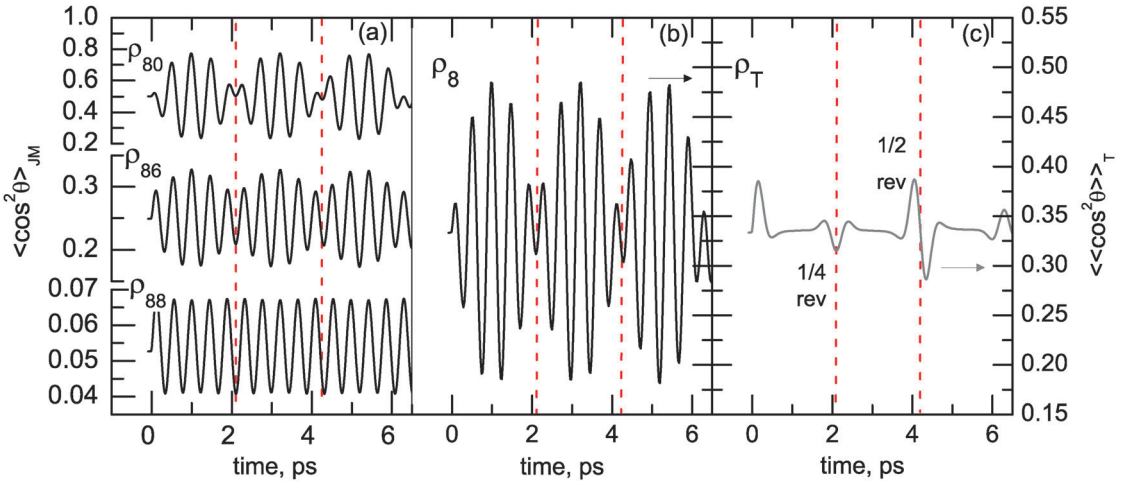

Fig. 4 (a) Numerical simulation of wave packet dynamics in the ρ_{80}, ρ_{86}, and ρ_{88} rotational states upon the excitation with a Gaussian laser pulse of 30 fs FWHM and a power density of 50 TW cm^{-2}. (b) Direction averaged densities ρ_8 under the same conditions. (c) Thermally averaged density packet ρ_T with weighting of states corresponding to 80 K. In all parts, the first quarter and half revival times are marked by vertical dashed lines.

The value of $\langle\cos^2\theta\rangle_{JM}$ in the $J \rightarrow J+2$ transition is increased beyond p^0_{JM} (Fig. 2), while the value of $\langle\cos^2\theta\rangle_{JM}$ in the $J \rightarrow J-2$ transition is decreased. The overall dynamics of the wave packet can be decomposed into two counter-propagating and thus beating parts.

For the ρ_{88} rotational wave packet, the coupling to the $J-2$ rotational level is forbidden, as $M > J-2$. The resulting dynamics, displayed in the lower trace in Fig. 4(a), are sinusoidal with the single frequency corresponding to the $J = 8 \rightarrow 10$ rotational transition. The directional average ρ_8 in Fig. 4(b) retains the characteristic beating amplitude, as for most of its M-substates the coupling to lower rotational levels is possible.

The ensemble average of the alignment at a temperature of 80 K is displayed in Fig. 4(c). It shows a pronounced half revival peak at $\tau_{1/2} = \hbar/(4B) = 4.18$ ps and a smaller feature at $\tau_{1/4} = \hbar/(8B) = 2.1$ ps. This quarter revival is particular for homonuclear molecules and originates from the imperfect cancellation of contributions from even and odd rotational states due to the different statistical weights in the thermal distribution.[41] In the individual rotational levels, the quarter revivals appear with the same amplitude as full and half revivals.[42]

The times for the first quarter and first half revivals are highlighted in the time traces of Fig. 4 by dashed vertical lines. Where both aligning and anti-aligning transitions are present, the curves for the individual wave packets in Fig. 4(a) display a remarkably low amplitude of alignment at the revival times. This is due to the mutual cancellation caused by the counter-propagating $\Delta J = +2$ and $\Delta J = -2$ parts. High values of alignment are reached at intermediate times. This alignment, however, is averaged out in the ensemble averaged $\langle\langle\cos^2\theta\rangle\rangle_T$, which explains the strong decrease of alignment amplitude in the revivals upon heating.[23,43] At high temperature, a large fraction of molecules is thermally rotationally excited, and transitions occur to both the lower and the higher lying rotational states. The higher the original J rotational level, the more substates can make an anti-Stokes transition and the more complete is the mutual cancellation of alignment and anti-alignment around the revival times.

4. Pulse duration effects

The rotational motion of a molecule is a slow process, compared to the timescales of vibrational or electronic dynamics. Rotational transition energies are small, resulting in a broad range of states populated even at low temperature. Typical revival times in the rotational wave packet motion of an ensemble of diatomic molecules range from a few picoseconds for light molecules, *e.g.* $\tau_{rev} = 8.38$ ps for nitrogen, to hundreds of picoseconds for heavy molecules, *e.g.* $\tau_{rev} = 450$ ps for the heavy iodine. At these times, the superposition of all excited rotations leads to the appearance of an overall anisotropy in the sample. The revival time τ_{rev} for a particular species is governed by the least common multiple of all rotational times associated with the excited transitions.[44] For rotational Raman transitions in the presence of a linearly polarized field with the selection rules $\Delta J = 0, \pm 2$, $\Delta M = 0$ this is given by the inverse of twice the rotational constant of the molecule, $\tau_{rev} = \hbar/(2B)$. The large number of states populated in a thermal ensemble and the quadratic dependence of the rotational energy on the J quantum number, however, result in a distribution of rotational times for individual transitions that at room temperature typically spans more than an order of magnitude. In a recent article we showed that the upper limit for non-adiabatic interaction is given by a laser pulse duration of about one tenth of the molecular rotational period.[25] For longer pulses, a notable decrease in the amplitude of the post-pulse alignment is observed. For the important nitrogen molecule and a typical Ti:sapphire laser pulse of 30 fs full width at half maximum (FWHM) duration the partly adiabatic regime is reached already for the $J = 12 \rightarrow 14$ rotational Raman transition.[25] At room temperature, molecules occupying rotational levels with $J \geq 12$ comprise about a quarter of the total population, see Fig. 1. The pulse duration of 150 fs FWHM of the common Ti:sapphire amplified fiber oscillators exceeds the strictly non-adiabatic limit in nitrogen for all except the $J = 0 \rightarrow 2$ rotational transitions. The segregation into adiabatic and non-adiabatic parts with the rotational distribution is therefore expected to play an important role under standard experimental conditions.

4.1 Interaction with a weak laser pulse

In the non-adiabatic limit of alignment the laser pulse is significantly shorter than the rotational period of the particular transitions excited in the molecule. As opposed to the adiabatic case, the field is turned off too fast to allow for a coherent de-excitation, and the common phase imprinted on the excited rotational transitions gives rise to wave packet oscillations. Within the non-adiabatic limit, laser pulses with equal time-integrated power densities should create equal post-pulse alignment.[25] In the previous paragraph we argued that the strictly non-adiabatic limit is easily exceeded under normal experimental conditions. Now we proceed to investigate the influence of laser pulse duration on the amplitude of the post-pulse alignment in rotational wave packets.

Within the approximation of an undepleted two-level system, the response of a quantum state to a perturbation is described by a sinusoidal oscillation at the beating frequency ω of the eigenenergies of the two levels.[45] In case of a laser pulse with finite duration, the time-dependent dynamics is given by a convolution of the oscillatory system response and laser pulse envelope. In case of a Gaussian laser pulse characterized by a FWHM duration τ_p this can be evaluated analytically and leads to oscillatory post-pulse dynamics at the transition frequency with the amplitude determined by the squared ratio of pulse duration to transition period.[25]

For a rotational Raman transition between the levels J' and J'' the transition frequency is denoted as $\omega_{J'\rightarrow J''}$, and the corresponding transition period is given by $\tau_{J'\rightarrow J''} = 2\pi/\omega_{J'\rightarrow J''}$. The convolution of rotational response and pulse envelope is thus expressed as

$$\rho_{J'M'J''M'}(t) \propto \int_{-\infty}^{\infty} \exp\left(-4\ln 2\frac{t'^2}{\tau_p^2}\right)\sin(\omega_{J'\rightarrow J''}(t-t'))\mathrm{d}t'$$
$$= \exp\left(-\frac{\pi^2}{4\ln 2}\frac{\tau_p^2}{\tau^2_{J'\rightarrow J''}}\right)\sin(\omega_{J'\rightarrow J''}t). \quad (19)$$

For the rotational transitions allowed for a thermally excited molecule, the possible transition frequencies and periods are given according to eqn (17) and (18) by $\omega_+ = -B(4J + 6)$ and $\tau_+ = 2\pi/\omega_+$ for $\Delta J = +2$, and by $\omega_- = B(4J - 2)$ and $\tau_- = 2\pi/\omega_-$ for the $\Delta J = -2$ transition, which is allowed for all states with $M \leq J - 2$. In case both transitions are allowed, the mean alignment scales with the pulse duration as

$$\langle \cos^2\theta \rangle_{JM}(t) \propto p^0_{JM} + p^+_{JM} \exp\left(-\frac{\pi^2}{4\ln 2}\frac{\tau_p^2}{\tau_+^2}\right)\sin(\omega_+ t) + p^-_{JM} \exp\left(-\frac{\pi^2}{4\ln 2}\frac{\tau_p^2}{\tau_-^2}\right)\sin(\omega_- t), \quad (20)$$

where p^0_{JM} is the mean alignment of ρ_{JM}, and p^+_{JM} and p^-_{JM} are transition probabilities according to eqn (11) and (12).

Eqn (19) and (20) show that the post-pulse amplitude of coherent oscillations depends on the ratio of the pulse duration to rotational period. For long pulses, the amplitude is exponentially dampened with a damping constant $\pi^2\tau_p^2/(4\ln 2\tau^2_{J'\to J''})$. For rotational periods at least an order of magnitude slower than the laser pulse duration, the interaction can be classified as non-adiabatic, while the adiabatic limit is reached as soon as the laser pulse duration starts exceeding the rotational period.

With differing ratios of p^+_{JM} and p^-_{JM} (Fig. 3), the transition from the non-adiabatic to the adiabatic limit is expected to show a dependence on the M quantum number. As τ_- is always larger than τ_+, the anti-Stokes, and thus anti-aligning, contribution is less dampened than the Stokes counterpart. Fig. 5 shows a plot of the oscillatory component of the post-pulse amplitude of alignment normalized to its value in the non-adiabatic limit *versus* the laser pulse duration for the ρ_{80}, ρ_{86}, and ρ_{88} rotational wave packets. The amplitude in the ρ_{88} rotational wave packet decreases faster than either of the two wave packets with both J-increasing and -decreasing oscillations, with the ρ_{86} packet showing a faster decrease than ρ_{80}. The post-pulse amplitude of the ρ_{88} wave packet follows almost ideally the curve given by eqn (19). The decay is given by $\exp[-\pi^2\tau_p^2/(4\ln 2\tau^2_{J=8\to 10})]$, and is represented in the figure by a solid line. The normalized amplitudes of the ρ_{80} wave packet are adequately described by substituting the frequency of the $J = 8 \to 6$ rotational transition into eqn (19), represented by the dotted line in the figure.

The decrease of the amplitude of the post-pulse alignment is thus influenced by effects of rotational frequency as well as effects of directionality. The rotational periods of the two possible transitions set the limits for the non-adiabatic to adiabatic transitions, while the localization of a particular ρ_{JM} wave packet in this transition area is determined by its M quantum number.

4.2 Interaction with an intense laser pulse

After the interaction with an intense laser pulse, the final rotational density of a molecule is described by a superposition of many rotational levels, which are populated by sequential Raman transitions from the original $|J,M\rangle$ state. The phase shift between the corresponding oscillations and a significant transfer of population between rotational levels makes it difficult to apply the semi-empirical model (eqn (19) and (20)) described above. A weak pulse would couple only the original rotational state and the two neighboring levels, while during the interaction with a strong pulse multiple levels are accessed sequentially, introducing a time delay between the oscillations associated with every individual transition. In the case of non-adiabatic laser pulses of weak and moderate power density, we found that the coherences created by laser pulses with equal integrated power density are identical.[25] Fig. 6(a) shows the J distribution resulting from the excitation of the $|J = 8, M = 0\rangle$ rotational level with a strong laser pulse of 30 fs FWHM duration and a power density of 50 TW cm^{-2}, with the time axis corresponding to $\pm 5\sigma$. Here, we select the $M = 0$ substate because in this case directionality effects are irrelevant as $p^+_{J0} \approx p^-_{J0}$ (Fig. 3). A broad distribution of rotational levels is populated after the termination of the pulse. In Fig. 6(b) the magnitude of the population of the rotational levels after the termination of the pulse is displayed for the pulse of Fig. 6(a) (green squares) and various laser pulses of different duration but identical integrated power density. On the side of low J levels, as in the case of a weak pulse, the distribution of population is similar for equal integrated power density. For short pulses, this is true also for the J-increasing transitions. Note that as expected from the transition probabilities displayed in Fig. 3 for $M = 0$, the $J + 2$ and $J - 2$ rotational states are populated with almost equal probability. This is not true for cases other than $M = 0$, where the J-increasing transition is favored by better overlap.

For longer pulses, however, one observes on the J-increasing side a less efficient transfer of population. The higher the excited level, the more short pulses are favored, and the population of higher excited and faster oscillating rotational levels is notably reduced with increasing pulse duration. This behavior is caused by the non-adiabatic to adiabatic transition, which depends on the particular rotational frequency, see Fig. 5. This is an effect independent of the directionality, as it is governed only by the ratio of rotational period of the particular transition and laser pulse duration. If during the interaction with a strong laser pulse rotational ladder climbing leads to the population of multiple rotational levels, the different frequencies associated with the transitions cause shifting of the onset of the non-adiabatic to adiabatic transition over the individual components of a wave packet originating from a single $|J,M\rangle$ state.

Fig. 7 shows the population of rotational levels in the ρ_{80} rotational wave packet upon excitation with a laser pulse of 0.5 ps FWHM, which is on the border of the adiabatic limit for the $J = 8$ rotational level. The time axis corresponds to $\pm 5\sigma$ of the laser pulse. The rotational periods associated with the $J = 8 \to 10$ and $J = 8 \to 6$ rotational transitions are 0.441 and 0.559 ps, respectively. In part (a) of Fig. 7, the case of a weak laser pulse of 5 TW cm^{-2} is displayed. In this case, the dynamics is adiabatic for the Stokes-transition, with the population being completely transferred back with the trailing edge of the pulse from the $J = 10$ rotational level, and almost adiabatic with some remaining population in the $J = 6$ rotational level for the anti-Stokes transition.

Fig. 7(b) shows excitation with a strong laser pulse of 50 TW cm^{-2}. During the interaction, many rotational states are populated through rotational ladder climbing. The post-pulse

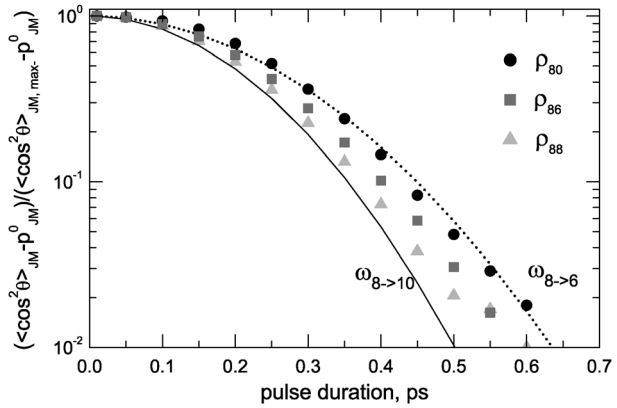

Fig. 5 M-dependence of the transition from non-adiabatic to adiabatic regime. The amplitude of the post-pulse alignment normalized to the non-adiabatic limit is plotted *versus* the FWHM duration of a Gaussian laser pulse with constant integrated power density corresponding to 50 TW cm^{-2} for 30 fs FWHM for the ρ_{80}, ρ_{86}, and ρ_{88} rotational wave packets. The lines represent the transition according to eqn (19) with the period of the rotational transitions $J = 8 \rightarrow 10$ (solid), and $J = 8 \rightarrow 6$ (dotted).

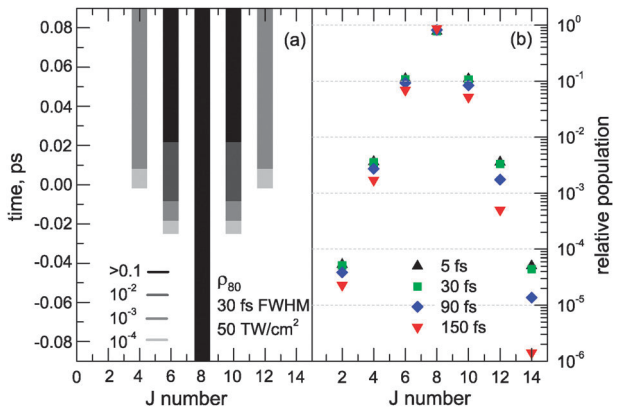

Fig. 6 (a) Logarithmic contour plot of the population of J rotational levels with the example of the ρ_{80} rotational wave packet upon the excitation with a Gaussian laser pulse of 30 fs FWHM duration and a power density of 50 TW cm^{-2}. (b) Semilogarithmic plot of the relative population of J levels at $t > t_f$ upon the excitation of the $|J = 8, M = 0\rangle$ state with laser pulse of various durations with integrated power density corresponding to the pulse in (a).

population, however, is determined by the non-adiabatic to adiabatic transition, which depends on the particular period of the oscillations. The population created at the high energetic side with high rotational frequency in the $J = 10$ to $J = 16$ rotational levels is largely transferred back with the trailing edge of the pulse. The slowly oscillating transitions to the lower rotational states already fall into the transition regime to the non-adiabatic case and do not respond in the same way to the trailing edge. A large part of the population transferred there is retained after the turn-off of the pulse. Note that this corresponds to a decrease in mean rotational energy upon the interaction with a strong laser pulse. Similar behavior is observed in all M states, with the condition of $\Delta M = 0$ limiting the accessible lower lying rotational levels.

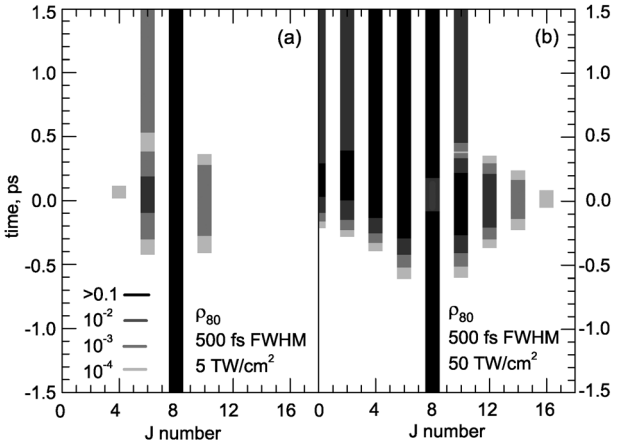

Fig. 7 Contour plot of the population of J rotational levels with the example of the ρ_{80} rotational wave packet upon excitation with a Gaussian laser pulse of 0.5 ps FWHM duration and a power density of 5 TW cm^{-2} (a) and 50 TW cm^{-2} (b).

5. Rotational heating *vs.* rotational cooling

The results of the above two sections show how J and M quantum numbers influence the molecular alignment in different ways. The state of rotational excitation, J, sets the overall time scale for non-adiabatic or adiabatic interaction through the rotational transition periods. The M quantum number determines whether along with absorption also stimulated emission of energy is allowed, and the relative contributions of each. Depending on the M state, thus two partial wave packets displaying aligning and anti-aligning motion can be created by the interaction with a linearly polarized laser pulse. Here, the transition matrix elements $p^{\pm}_{JM}$ favor a J-increasing transition for $M \approx J$, and tend to equal values for $J \gg M$.

The transition from the non-adiabatic to the adiabatic regime depends on the ratio of rotational period and laser pulse duration, and thus is faster on the high J-side of the rotational distribution. For increasing laser pulse duration the rotational energy is more efficiently removed from the aligning than from the anti-aligning part of the rotational wave packet by the trailing edge of the laser pulse. Fig. 7 exemplifies this for fixed pulse duration and two different powers. In order to determine to what extent the rotational energy of the wave packet can be influenced by such effects, we performed numerical simulations for the $|J = 8, M = 0\rangle$ state over a range of pulse durations between 0.01 and 0.6 ps and pulse powers between 1 and 100 TW cm^{-2}. Fig. 8 shows surface plots of the rotational energy, represented by the expectation value of $\langle J(J + 1)\rangle$, *versus* laser pulse power and duration for the ρ_{80}, ρ_{86}, and ρ_{88} rotational wave packets and the directional average ρ_8. The expectation value $\langle J(J + 1)\rangle$ for the $J = 8$ rotational level is 72. Values close to this between 70 and 75 are displayed in the figure as a gray area. Higher values are represented by contour lines of darker color, and lower values by lighter color. In Fig. 8(a) for the ρ_{80} rotational wave packet for short laser pulses up to a power density of 40 TW cm^{-2} no significant change in the rotational energy is visible. Above this power density, an increase in rotational energy can be observed. An increase in the mean rotational energy corresponds to

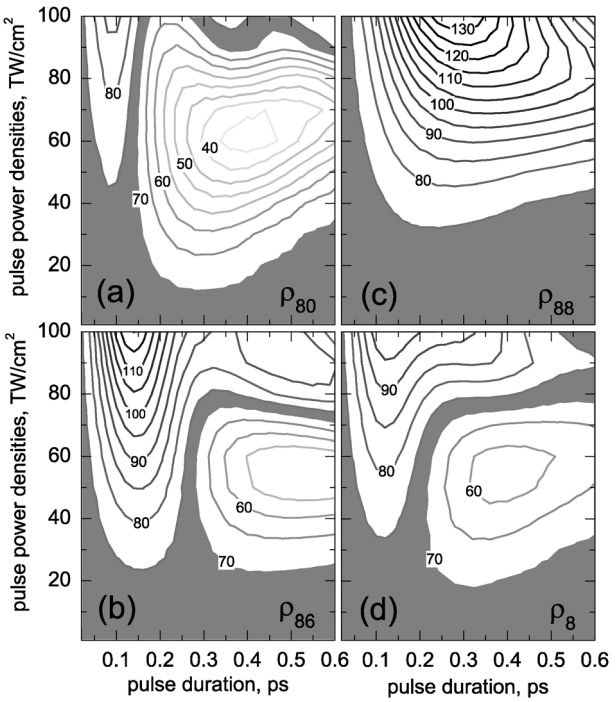

Fig. 8 Expectation value of $J(J + 1)$, as a measure of rotational energy, as a function of laser pulse duration and power density for the (a) ρ_{80}, (b) ρ_{86}, and (c) ρ_{88} rotational wave packets, and the M-averaged ρ_8 density packet in (d). The gray area corresponds to $70 < J(J + 1) < 75$, with the value for the initial $J = 8$ being 72.

heating of the rotational degrees of freedom. Going to longer pulse duration, however, there appears at a pulse duration of about 0.15 ps, corresponding to about one third of the rotational period, an almost vertical line marking a region with no net transfer of energy. For shorter pulses, $\langle J(J + 1)\rangle$ is increasing, but on the side of longer pulse duration the dominating effect is a decrease in the rotational energy, or rotational cooling. It reaches a minimum for a pulse with a power density of 60 TW cm^{-2} and a duration of 400–450 fs. In this region the rotational energy is reduced by half compared to its original value.

A quite similar structure can be observed for the ρ_{86} rotational wave packet with a vertical border at 0.25 ps pulse duration separating the region with preferred rotational heating from the one with preferred rotational cooling independently of the pulse power (Fig. 8(b)) up to a power of about 70 TW cm^{-2}. Here, the region of rotational heating is larger than in the case of ρ_{80}, as expected from the transition probabilities of Fig. 3. For the ρ_{88} wave packet in Fig. 8(c), the emission of energy is forbidden due the requirement of M conservation, and thus the surface shows the expected increase in mean energy with pulse power and pulse duration up to the onset of the adiabatic regime. The M-averaged values for ρ_8 in Fig. 8(d) yield a region with preferred heating for short pulses and very high power, and a region with preferred cooling for long pulses of moderate to high power.

This change in rotational energy is expected to influence the post-pulse alignment observed in the particular wave packets. In Fig. 9 we plot the relative deviation of the time-averaged post-pulse alignment $\overline{\langle\cos^2\theta\rangle}_{JM}$ from the value of p^0_{JM} given by eqn (10) for pulse durations between 0.01 and 0.6 ps and a constant power density of 50 TW cm^{-2} for the densities of Fig. 8. The time-averaged post-pulse alignment is a measure for the overall anisotropy created in the sample by the laser pulse. It corresponds to the population part of alignment, as defined in, *e.g.*, ref. 46. The curves show behavior expected from the transfer of energy surface of Fig. 8, with the ρ_{80} and ρ_{86} wave packets displaying a decrease in alignment for all but the shortest pulses, and the ρ_{88} wave packet showing an increase. In all cases one observes a maximum or minimum, respectively, after which the transition to the adiabatic limit tends to reduce the post-pulse anisotropy to zero.

The inset of Fig. 9 shows the time-dependent alignment dynamics $\langle\cos^2\theta\rangle(t)$ in the ρ_{80} wave packet in response to a laser pulse of 0.5 ps FWHM duration and a power density of 50 TW cm^{-2}. The coherent superposition of rotational transition gives rise to an oscillatory post-pulse alignment pattern. While the laser pulse is on, the molecule is forced into anti-alignment, as expected from the net transfer of energy out of the molecules shown in Fig. 7.

From Fig. 8(a) and (b) it is obvious that the rotational energy is decreased more efficiently in the $M = 0$ case than in the case of $M = 6$. In Fig. 9, however, $\overline{\langle\cos^2\theta\rangle}_{86}$ shows a much more pronounced decrease than $\overline{\langle\cos^2\theta\rangle}_{80}$. The average anisotropy is thus not only related to the overall amount of rotational energy in the wave packet but also to the M quantum number of the states. Indeed, Fig. 2 shows that the change in alignment upon a rotational transition depends on J and on M, a rotational transition where JM does not lead to any notable change in alignment. In the case of Fig. 9, this is best fulfilled by the ρ_{80} wave packet, which does indeed show a relatively small change in average alignment despite a large change in rotational energy. The alignment decrease is more pronounced in the case of ρ_{86}, which in comparison loses less energy to the pulse.

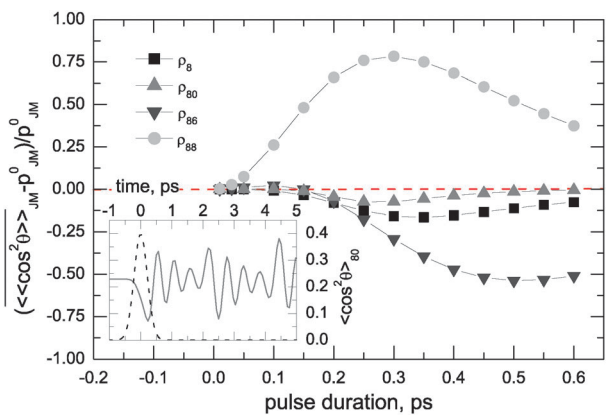

Fig. 9 Relative deviation from p^0_{JM} of the time-averaged post-pulse alignment $\overline{\langle\cos^2\theta\rangle}_{JM}$ for the ρ_{80}, ρ_{86}, and ρ_{88} rotational wave packets and the M-average ρ_8. The inset shows the time-dependent alignment of ρ_{80} upon excitation with a Gaussian laser pulse of 0.5 ps FWHM duration and a power density of 50 TW cm^{-2}.

6. Conclusions

In this article, we examined the influence of directionality and pulse duration on the rotational alignment of rotationally excited molecules. Molecules in rotationally excited states can interact with a laser pulse not only by absorbing energy but also by stimulated emission, leading to rotational heating or cooling, respectively. The extent to which these processes are present in the interaction depends on one hand *via* the M quantum number on the directionality of the molecular angular momentum, and on the other hand *via* the particular transition frequencies to higher and lower lying rotational states also on the pulse duration. The transition to higher rotational levels corresponds to an aligning motion of the molecule, and the transition to lower rotational levels to an anti-aligning motion. A semi-empirical approach combining two two-state models can qualitatively account for the shape and amplitude of post-pulse alignment induced by a laser pulse of moderate power density. With increasing J number, a decreasing amplitude of alignment at the rotational revival times is observed due to the mutual cancellation of aligning and anti-aligning dynamics. At high laser power, rotational ladder climbing and a phase shift accumulating between oscillatory components causes deviations from this simple behavior. The difference in the frequencies associated with the respective rotational transitions leads to the possibility of the faster oscillating aligning part of the wave packet being more affected by the laser pulse duration than the anti-aligning part. While it is generally expected that photo-induced alignment leads to rotational heating, we have shown that for a wide range of laser pulse duration and energy, a region is created in which rotational cooling, and thus post-pulse anti-alignment, prevail over rotational heating, or post-pulse alignment.

Acknowledgements

The authors thank M. Héjjas, F. Königsmann and Dr R. Püttner for fruitful and constructive discussions. Financial support from Deutsche Forschungsgemeinschaft *via* Sonderforschungsbereich 450 is gratefully acknowledged.

References

1 H. Stapelfeldt and T. Seideman, *Rev. Mod. Phys.*, 2003, **75**, 543.
2 Y. Ohshima and H. Hasegawa, *Int. Rev. Phys. Chem.*, 2010, **29**, 619.
3 T. Seideman and E. Hamilton, *Adv. At., Mol., Opt. Phys.*, 2006, **52**, 289.
4 B. Friedrich and D. Herschbach, *Phys. Rev. Lett.*, 1995, **74**, 4623.
5 B. Friedrich and D. Herschbach, *J. Phys. Chem.*, 1995, **99**, 15686.
6 J. Ortigoso, M. Rodriguez, M. Gupta and B. Friedrich, *J. Chem. Phys.*, 1999, **110**, 3870.
7 M. Leibscher and B. Schmidt, *Phys. Rev. A: At., Mol., Opt. Phys.*, 2009, **80**, 012510.
8 T. Seideman, *Phys. Rev. Lett.*, 1999, **83**, 4971.
9 F. Rosca-Pruna and M. J. J. Vrakking, *Phys. Rev. Lett.*, 2001, **87**, 153902.
10 R. de Nalda, E. Heesel, M. Lein, N. Hay, R. Velotta, E. Springate, M. Castillejo and J. P. Marangos, *Phys. Rev. A: At., Mol., Opt. Phys.*, 2004, **69**, 031804.
11 I. V. Litvinyuk, K. F. Lee, P. W. Dooley, D. M. Rayner, D. M. Villenneuve and P. B. Corkum, *Phys. Rev. Lett.*, 2003, **90**, 233003.
12 P. Dooley, I. V. Lityinyuk, K. F. Lee, D. M. Rayner, M. Spanner, D. M. Villeneuve and P. B. Corkum, *Phys. Rev. A: At., Mol., Opt. Phys.*, 2003, **68**, 023406.
13 J. Itatani, J. Levesque, D. Zeidler, H. Niikura, H. Pepin, J. C. Kieffer, P. B. Corkum and D. M. Villeneuve, *Nature*, 2004, **432**, 867.
14 T. Kanai, S. Minemoto and H. Sakai, *Nature*, 2005, **435**, 470.
15 R. Torres, N. Kajumba, J. G. Underwood, J. S. Robinson, S. Baker, J. W. G. Tisch, R. de Nalda, W. A. Bryan, R. Velotta, C. Altucci, I. C. E. Turcu and J. P. Marangos, *Phys. Rev. Lett.*, 2007, **98**, 203007.
16 B. K. McFarland, J. P. Farrell, P. H. Bucksbaum and M. Gühr, *Science*, 2008, **322**, 1232.
17 L. Holmegaard, J. H. Nielsen, I. Nevo, H. Stapelfeldt, F. Filsinger, J. Küpper and G. Meijer, *Phys. Rev. Lett.*, 2009, **102**, 023001.
18 O. Ghafur, A. Rouzee, A. Gijsbertsen, W. K. Siu, S. Stolte and M. J. J. Vrakking, *Nat. Phys.*, 2009, **5**, 289.
19 N. Owschimikow, F. Königsmann, J. Maurer, P. Giese, A. Ott, B. Schmidt and N. Schwentner, *J. Chem. Phys.*, 2010, **133**, 044311.
20 M. Leibscher, I. S. Averbukh and H. Rabitz, *Phys. Rev. Lett.*, 2003, **90**, 213001.
21 M. Leibscher, I. Averbukh and H. Rabitz, *Phys. Rev. A: At., Mol., Opt. Phys.*, 2004, **69**, 013402.
22 M. Lemeshko and B. Friedrich, *J. Phys. Chem. A*, 2010, **114**, 9848.
23 R. Torres, R. de Nalda and J. P. Marangos, *Phys. Rev. A: At., Mol., Opt. Phys.*, 2005, **72**, 023420.
24 F. Rosca-Pruna and M. J. J. Vrakking, *J. Chem. Phys.*, 2002, **116**, 6579.
25 N. Owschimikow, B. Schmidt and N. Schwentner, *Phys. Rev. A: At., Mol., Opt. Phys.*, 2009, **80**, 053409.
26 H. Hasegawa and Y. Ohshima, *Phys. Rev. A: At., Mol., Opt. Phys.*, 2006, **74**, 061401.
27 H. Hasegawa and Y. Ohshima, *Phys. Rev. Lett.*, 2008, **101**, 053002.
28 M. Fischer, U. Lorenz, B. Schmidt and R. Schmidt, *Phys. Rev. A*, submitted.
29 G. Herzberg, *Molecular Spectra and Molecular Structure. I. Spectra of Diatomic Molecules*, Krieger Publishing Company, Malabar, FL, reprint edn, 1989.
30 M. P. Bogaard, A. D. Buckingham, R. K. Pierens and A. H. White, *J. Chem. Soc., Faraday Trans. 1*, 1978, **74**, 3008.
31 V. Loriot, E. Hertz, A. Rouzee, B. Sinardet, B. Lavorel and O. Faucher, *Opt. Lett.*, 2006, **31**, 2897.
32 V. Loriot, E. Hertz, B. Lavorel and O. Faucher, *J. Phys. B: At., Mol. Opt. Phys.*, 2008, **41**, 015604.
33 B. Schmidt and U. Lorenz, *U Lorenz*, 2009, WavePacket 4.7: A program package for quantum-mechanical wavepacket propagation and time-dependent spectroscopy. Available *via* http://wavepacket.sourceforge.net.
34 S. Mukamel, *Nonlinear Optical Spectroscopy*, Oxford University Press, Oxford, 1995.
35 B. I. Grimberg, V. V. Lozovoy, M. Dantus and S. Mukamel, *J. Phys. Chem. A*, 2002, **106**, 697.
36 E. J. Brown, Q. Zhang and M. Dantus, *J. Chem. Phys.*, 1999, **110**, 5772.
37 V. Renard, M. Renard, S. Guerin, Y. T. Pashayan, B. Lavorel, O. Faucher and H. R. Jauslin, *Phys. Rev. Lett.*, 2003, **90**, 153601.
38 H. Stapelfeldt, E. Constante and P. B. Corkum, *Phys. Rev. Lett.*, 1995, **74**, 3780.
39 P. W. Atkins and R. S. Friedman, *Molecular Quantum Mechanics*, Oxford University Press, Oxford, 3rd edn, 1999.
40 R. Zare, *Angular Momentum: Understanding Spatial Aspects in Chemistry and Physics*, Wiley, New York, 1988.

41 I. S. Averbukh and N. F. Perelman, *Phys. Lett. A*, 1989, **139**, 449.
42 S. Fleischer, I. S. Averbukh and Y. Prior, *Phys. Rev. Lett.*, 2007, **99**, 093002.
43 Z. Q. Yang and X. X. Zhou, *Acta Phys.-Chim. Sin.*, 2006, **22**, 932.
44 R. W. Robinett, *Phys. Rep.*, 2004, **392**, 1.
45 J. I. Steinfeld, *Molecules and Radiation: An Introduction to Modern Molecular Spectroscopy*, Dover, Mineola, NY, 2nd edn, 2005.
46 S. Ramakrishna and T. Seideman, *Phys. Rev. Lett.*, 2005, **95**, 113001.

